IOPscience iopscience.iop.org

Home Search Collections Journals About Contact us My IOPscience

Alpha-bungarotoxin binding to target cell in a developing visual system by carboxylated nanodiamond

This content has been downloaded from IOPscience. Please scroll down to see the full text.

2008 Nanotechnology 19 205102

(http://iopscience.iop.org/0957-4484/19/20/205102)

View the table of contents for this issue, or go to the journal homepage for more

Download details:

IP Address: 140.113.38.11
This content was downloaded on 25/04/2014 at 16:10

Please note that terms and conditions apply.

Nanotechnology **19** (2008) 205102 (10pp) doi:10.1088/0957-4484/19/20/205102

Alpha-bungarotoxin binding to target cell in a developing visual system by carboxylated nanodiamond

Kuang-Kai Liu[1,2,3], Mei-Fang Chen[4], Po-Yi Chen[1,2,4], Tony J F Lee[1,2,5], Chia-Liang Cheng[6], Chia-Ching Chang[3,7], Yen-Peng Ho[8] and Jui-I Chao[1,2,3,9]

[1] Institute of Pharmacology and Toxicology, Tzu Chi University, Hualien 970, Taiwan
[2] Biomedical Nanotechnology Laboratory, Tzu Chi University, Hualien 970, Taiwan
[3] Department of Biological Science and Technology, National Chiao Tung University, Hsin-Chu 300, Taiwan
[4] Neuro-Medical Scientific Center, Tzu Chi General Hospital, Hualien 970, Taiwan
[5] Department of Pharmacology, School of Medicine, Southern Illinois University, Springfield, IL, USA
[6] Department of Physics, National Dong Hwa University, Hualien 974, Taiwan
[7] Institute of Physics, Academia Sinica, Taipei 11529, Taiwan
[8] Department of Chemistry, National Dong Hwa University, Hualien 974, Taiwan

E-mail: chaoji@mail.tcu.edu.tw

Received 22 November 2007, in final form 17 March 2008
Published 14 April 2008
Online at stacks.iop.org/Nano/19/205102

Abstract

Biological molecules conjugating with nanoparticles are valuable for applications including bio-imaging, bio-detection, and bio-sensing. Nanometer-sized diamond particles have excellent electronic and chemical properties for bio-conjugation. In this study, we manipulated the carboxyl group produced on the surface of nanodiamond (carboxylated nanodiamond, cND) for conjugating with alpha-bungarotoxin (α-BTX), a neurotoxin derived from *Bungarus multicinctus* with specific blockade of alpha7-nicotinic acetylcholine receptor (α7-nAChR). The electrostatic binding of cND–α-BTX was mediated by the negative charge of the cND and the positive charge of the α-BTX in physiological pH conditions. Sodium dodecyl sulfate-polyacrylamide gel analysis and matrix-assisted laser desorption ionization time-of-flight mass spectrometry (MALDI/TOF-MS) spectra displayed that α-BTX proteins were conjugated with cND particles via non-covalent bindings. The green fluorescence of the cND particles combining with the red fluorescence of tetramethylrhodamine-labeled α-BTX presented a yellow color at the same location, which indicated that α-BTX proteins were conjugated with cND particles. *Xenopus laevis's* oocytes expressed the human α7-nAChR proteins by microinjection with α7-nAChR mRNA. The cND–α-BTX complexes were bound to α7-nAChR locating on the cell membrane of oocytes and human lung A549 cancer cells analyzed by laser scanning confocal microscopy. The choline-evoked α7-nAChR-mediated inward currents of the oocytes were blocked by cND–α-BTX complexes in a concentration-dependent manner using two-electrode voltage-clamp recording. Furthermore, the fluorescence intensity of cND–α-BTX binding on A549 cells could be quantified by flow cytometry. These results indicate that cND-conjugated α-BTX still preserves its biological activity in blocking the function of α7-nAChR, and provide a visual system showing the binding of α-BTX to α7-nAChR.

[9] Address for correspondence: Institute of Pharmacology and Toxicology, Tzu Chi University, 701, Section 3, Chung-Yang Road, Hualien 970, Taiwan.

 © 2008 IOP Publishing Ltd Printed in the UK

1. Introduction

Manipulating nanoparticles for biomedical applications has been evaluated in recent years [1–5]. Biological molecules conjugated with nanoparticles can be applied for both diagnostic and therapeutic applications [1, 2, 5, 6]. Semiconductor quantum dots (Qdots) display fluorescent properties without photobleaching that are suitable for advanced bioimaging [1, 3, 6]. For example, Qdot-coating with a lung-targeting peptide was specifically accumulated in the lung of mice by vessel injection [1]. The visual analysis of the delivery processes of nanoparticle-conjugated therapeutic drugs (or bio-molecules) *in vivo* provides the observation of drug transportation and targeting, which are useful for therapeutic efficacy of such diseases. Unfortunately, the existence of heavy metals such as cadmium (a well-known human toxicant) in Qdots is of concern for medical applications, especially for human treatment. Therefore, alternative nanomaterials containing both biocompatible and detectable properties are highly desirable.

Nanodiamond, a carbon derivative nanomaterial, is a developing nanoparticle for biological applications, which include the advantages of its biocompatibility, non-toxicity, and easily detected intrinsic fluorescence without photobleaching [7–9]. The surface of nanodiamonds provides an exceptional platform for conjugation of biological molecules after chemical modifications [10, 11]. The modified surface of nanodiamonds by carboxylation (carboxylated nanodiamond, cND) presents high affinity for proteins [7, 12]. Besides, the modified nanodiamonds can be conjugated with DNA [10, 13], cytochrome c [14], antigen [15], and growth hormone [16]. However, the biological activity and function of bio-molecules conjugated with cND are still unclear.

Alpha-bungarotoxin (α-BTX), a neurotoxin derived from *Bungarus multicinctus*, is an antagonist of the alpha7-nicotinic acetylcholine receptor (α7-nAChR) of neuronal cells by inducing neuronal damages [17, 18]. Non-neuronal cells (e.g., human lung cancer cells) also expressed α7-nAChR [19–21]. The α 7-nAChR forms a functional homomeric-pentamer nAChR on the cellular membrane to mediate cation (e.g. Ca^{2+}) influx that is activated by an agonist such as choline and nicotine [22–25]. It has been shown that α7-nAChR can regulate many physiological functions including cell proliferation [21, 26] and neuroprotection [17, 27].

In the present study, we manipulated the carboxyl group produced on the nanodiamond's surface for conjugating with α-BTX by imaging and binding to those α7-nAChR in *Xenopus laevis's* oocyte and lung cancer cell. The cND–α-BTX can be visualized on the targeting cells. Furthermore, the cND-conjugated α-BTX executes the biological function to block the activation of α7-nAChR.

2. Experimental details

2.1. Materials and reagents

The nominal 100 nm nanodiamond powder was from Diamond Innovations (Worthington, OH). α-BTX, α-BTX-tetramethylrhodamine (α-BTX-TMR), and ferulic acid were purchased from Sigma Chemical Co. (St Louis, MO). HPLC grade acetonitrile (MeCN) was purchased from J T Backer (Phillipsburg, NJ). Formic acid was purchased from Riedel-de Haen (Seelze, Germany). Water was purified using a Milli-Q system (Millipore, Bedford, MA).

2.2. A549 cancer cell line

A549 cell line (ATCC, #CCL-185) was derived from the lung adenocarcinoma of a 58 year-old Caucasian male. It has been shown that A549 cells expressed α7-nAChR proteins [19–21]. These cells were cultured in RPMI-1640 medium (Invitrogen Co., Carlsbad, CA), which were supplemented with 10% fetal bovine serum (FBS), 100 units ml^{-1} penicillin, 100 $\mu g\ ml^{-1}$ streptomycin, and L-glutamine (0.03%, w/v). The cells were maintained at 37 °C and 5% CO_2 in a humidified incubator (310/Thermo, Forma Scientific, Inc., Marietta, OH).

2.3. Preparation of cND–α-BTX and cND–α-BTX-TMR

The standard procedure of cND preparation was according to a previous study [14]. Briefly, 0.2 g 100 nm nanodiamond powder was added into a 15 ml acid mixture of H_2SO_4:HNO_3 (3:1) in an ultrasonic bath for incubation of 30 min, and then heated for 30 min. The treated nanodiamonds were washed with distilled water and centrifuged several times. After drying, these cND particles were dispersed in distilled water. For preparing cND–α-BTX and cND–α-BTX-TMR, the cND particles (50 mg ml^{-1}) were mixed with α-BTX (500 $\mu g\ ml^{-1}$) or α-BTX-TMR (500 $\mu g\ ml^{-1}$) in the shaker for 2 h at room temperature. The mixtures were centrifuged at 12 000 rpm for 5 min, and the pellets were washed twice with isotonic PBS (pH 7.4). Finally, the pellet was dissolved in PBS. These cND–protein complexes need to be freshly prepared. To avoid aggregation, the samples were ultrasonicated for 20 min at room temperature before use.

2.4. Measurement of particle sizes of α-BTX, cND, and cND–α-BTX

The particle size distributions of α-BTX, cND and cND–α-BTX were analyzed with a laser light scattering goniometer, BI-200 SM with Brookhaven BI-9000AT software (Brookhaven Instruments, Holtsville, New York, USA).

2.5. Bio-atomic force microscopy (Bio-AFM)

To examine the morphology and size of cNDs and cND–α-BTX complexes, these particles were dropped on a mica slice and were analyzed with a Bio-AFM (NanoWizard, JPK Instruments, Berlin). The Bio-AFM was mounted on an inverted microscope, TE-2000-U (Nikon, Japan). A silicon nitride non-sharpened cantilever was used with a nominal force constant of 0.06 N m^{-1} (DNP-20, Veeco). The images were scanned by using the contact mode. Line scan rates were varied from 0.5 to 2 Hz.

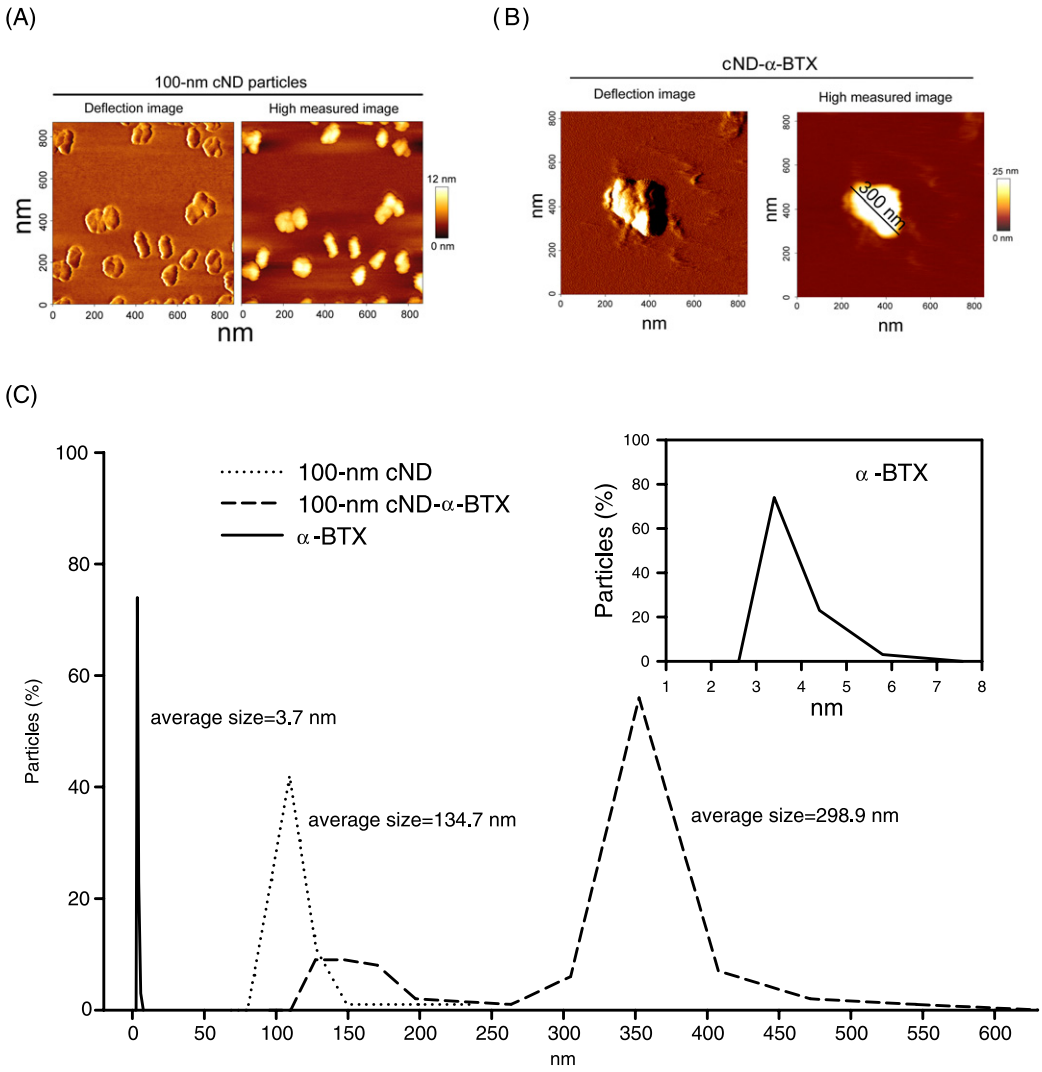

Figure 1. Size distributions of cND, α-BTX, and cND–α-BTX. (A) cND particles and (B) cND–α-BTX complexes were dropped on a mica slice and were analyzed with a Bio-AFM. The deflection image of the Bio-AFM shows the contour and size of cND particles and cND–α-BTX. (C) The particle size distributions of α-BTX, cND and cND–α-BTX were analyzed by a laser light scattering goniometer. The upper right image was amplified by the size distribution of α-BTX. The average sizes of molecules were calculated as shown in the figure.

2.6. Sodium dodecyl sulfate-polyacrylamide gel (SDS-PAGE) analysis

Briefly, the suspensions of cND, α-BTX, and cND-BTX were separately subjected to electrophoresis by 12% SDS-PAGE. The indicated molecular weight was loaded by a protein marker reagent (Cambrex, Maine). After electrophoresis, the gel was stained with the coomassie blue buffer (0.1% coomassie blue, 10% acetic acid, and 45% methanol) for 1 h.

2.7. MALDI/TOF-MS spectrometry

The cND–α-BTX particles were extensively washed with Milli-Q-filtered water. The supernatant obtained from every washing procedure was analyzed by MALDI/TOF-MS. MALDI/TOF-MS spectra were acquired using an Autoflex time-of-flight mass spectrometer (Bruker Daltonic, Germany) equipped with a 337 nm nitrogen laser (10 Hz, 3 ns pulse width). Spectral data were obtained in the linear mode with an acceleration voltage of 25 kV. Each mass spectrum was derived from 50 summed scans. Ferulic acid was used as a MALDI matrix, which was prepared by dissolving 12.5 mg of ferulic acid in 1 ml of solvent mixture of 17% formic acid/33% MeCN/50% H_2O. An aliquot of the sample solution (0.5 μl) was mixed with an equal volume of the matrix solution and then applied on the target plate and dried before MALDI/TOF-MS analysis.

2.8. Expression of a human α7-nAChR in Xenopus laevis's oocytes

Stage V and VI oocytes from *Xenopus laevis* were harvested and maintained in the modified ND96 buffer (96 mM NaCl, 2 mM KCl, 1 mM $MgCl_2$, 1.8 mM $CaCl_2$ and 5 mM HEPES, pH 7.6) at 18.5 °C. The human α7-nAChR plasmid was kindly provided by Dr Barry J Hoffer (National Institute on Drug Abuse, NIH, Baltimore). The mMessage mMachine kit (Ambion Inc.) was adopted to synthesize capped α7-nAChR

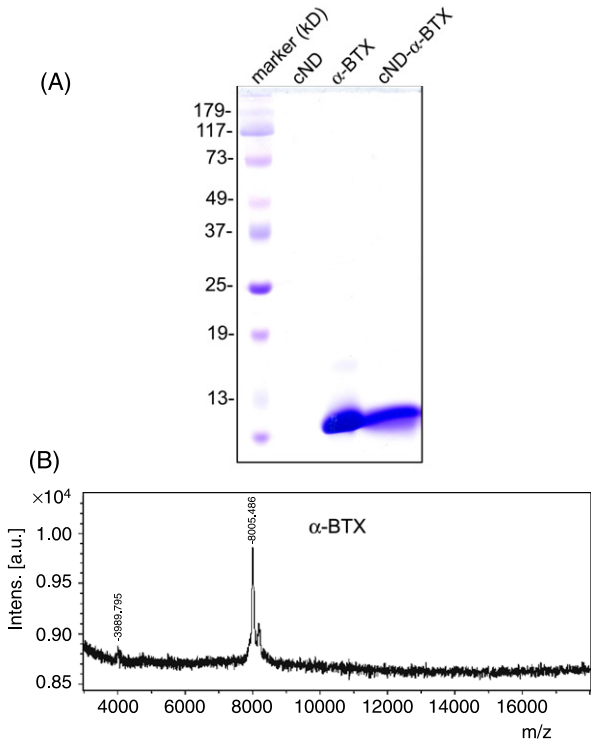

Figure 2. Detection of α-BTX by SDS-PAGE analysis and MALDI/TOF-MS spectrum. (A) The cND particles, α-BTX, and cND–α-BTX were subjected to electrophoresis by SDS-PAGE. Each well was loaded with 100 nm cNDs (500 μg ml^{-1}), α-BTX (20 μg), and 750 μg cND–α-BTX (containing 20 μg α-BTX), respectively. After electrophoresis, the gel was stained with the coomassie blue staining. The left lane indicates the protein marker. (B) The α-BTX protein was detected by MALDI/TOF-MS from the dissociation of cND–α-BTX particles. The peak at m/z 8005 corresponds to the α-BTX protein ion.

RNAs *in vitro*. Oocytes were injected with the α7-nAChR RNA by using a nanoinjector (Drummond, Inc., Broomall, PA).

2.9. Confocal microscopy

A549 cells were cultured on coverslips, which were kept in a 35 mm Petri dish for 16–20 h before treatment. After treatment with 100 μg ml^{-1} cNDs or cND–α-BTX for 4 h, the cells were washed twice with isotonic PBS (pH 7.4) and then were re-cultured in complete medium for 20 h. At the end of incubation, the cells were fixed in 4% paraformaldehyde solution in PBS for 1 h at 37 °C. Then the coverslips were washed three times with PBS, and non-specific binding sites were blocked in PBS containing 10% normal goat serum, 0.3% Triton X-100 for 1 h. The cytoskeleton of β-tubulin protein was stained with anti-β-tubulin Cy3 (1:50) for 30 min at 37 °C. Finally, the samples were examined under a Leica confocal laser scanning microscope (Mannheim, Germany) that was equipped with a UV laser (351/364 nm), an Ar laser (457/488/514 nm), and a HeNe laser (543 nm/633 nm).

The oocytes from *Xenopus laevis* were injected with human α7-nAChR RNA and then incubated for 2–7 days. After incubation, the vitelline membrane of oocytes was carefully removed. Thereafter, oocytes were carefully washed twice with the ND96 buffer before treatment with 100 μg ml^{-1} cNDs or cND–α-BTX for 10 min. At the end of treatment, the oocytes were washed with the ND96 buffer and then fixed with in 4% paraformaldehyde solution for 2 h. Subsequently, the oocytes were analyzed with a confocal laser scanning microscope.

2.10. Flow cytometry

A549 cells were plated at a density of 7×10^5 cells per 60 mm Petri dish in complete medium for 16–20 h. Thereafter, the cells were treated with 100 μg ml^{-1} cND or cND–α-BTX for 4 h. After treatment, the cells were washed twice with PBS and were re-cultured in complete medium for two days. The cells were collected and fixed with ice-cold 70% ethanol overnight at −20 °C. To avoid cell aggregation, the cell solutions were filtered through nylon membrane (BD Biosciences, San Jose, CA). Finally, the samples were analyzed with a flow cytometer (BD Biosciences). Ten thousand cells were analyzed, and the fluorescence intensity was quantified by a CellQuest software (BD Biosciences).

2.11. Two-electrode voltage-clamp recording

The main procedure of two-electrode voltage-clamp recording was described in a previous study [28]. Membrane currents were recorded 2–7 days after the injection. During recording, the oocyte was continuously perfused with the ND96 buffer at a rate of 7 ml min^{-1}. Choline (0.3 mM) was then applied for 1 s directly onto the oocyte. For examining the effects of cND, α-BTX, or cND-BTX on choline-induced responses, these molecules were dissolved in the ND96 buffer and flowed continuously into the bath chamber for 5 min. Choline responses were examined during treatments. After these molecules were 'washed off', the response to choline alone was repeated to obtain an additional control. Two-electrode voltage-clamp recording for the whole oocyte was performed at room temperature by using an OC-725C amplifier (Warner, Inc., Hamden, CT). The borosilicate glass capillaries (1.5 mm, outer diameter) (World Precision Instruments, Inc., Sarasota, FL) were pulled using a P-97 microelectrode puller (Sutter, Inc., Novato, CA). The electrodes were filled with 3 M KCl and had 0.1–1 MΩ resistance. The membrane potential was held at −60 mV. Data acquisition and analysis were performed with a Digidata 1322A and pClamp 9.0 (Axon instruments, Inc., Union City, CA). The traces were filtered at 1 kHz and sampled at 2 kHz. The maximal negative deflection of the current was determined as the current amplitude. To compensate the difference in the α7-nAChR expression level, the data were normalized to the current amplitudes before the drug administration and presented as percentages of the choline-induced response.

2.12. Statistical analysis

Data were analyzed using Student's t test, and a p value of <0.05 was considered as statistically significant in each experiment.

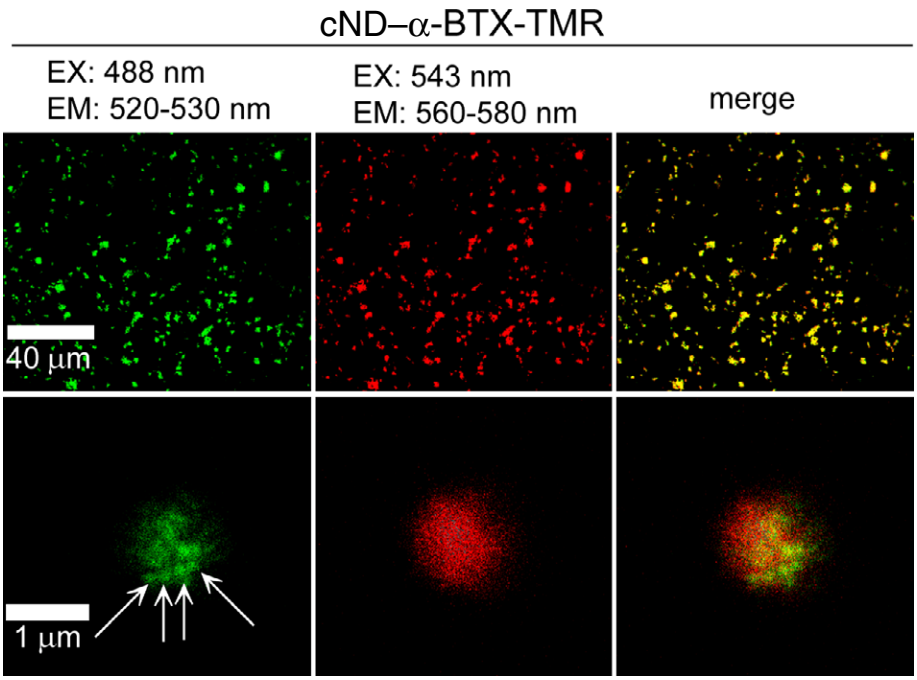

Figure 3. Detection of cND–α-BTX-TMR complexes by laser scanning confocal microscopy. The cND particles (750 μg) were incubated with α-BTX-TMR (15 μg). After incubation, the cND–α-BTX-TMR complexes were subjected to laser scanning confocal microscopy. The green fluorescence from the cNDs was excited with wavelength 488 nm and the emission was collected in the range of 510–530 nm. Arrows indicate the location of cND particles. The red fluorescence of TMR was excited by the wavelength of 543 nm and then the emission at 560–580 nm was detected. The yellow color in the merged pictures shows cND–α-BTX-TMR complexes.

3. Results

3.1. Morphology and size of cND and cND–α-BTX

As shown in figure 1(A), the nominal size of 100 nm cND particles was ~100 nm. The morphology of cND particles was oblong under Bio-AFM observation (figure 1(A)). However, the size of the cND–α-BTX complex was increased to ~300 nm (figure 1(B)). Moreover, a laser light scattering goniometer was used to measure the size distribution of α-BTX, cND, and cND–α-BTX. The average sizes of α-BTX and cND were 3.7 and 134.7 nm, respectively (figure 1(C)). The cND particles conjugated with α-BTX and formed the cND–α-BTX complexes with average size 298.9 nm (figure 1(C)).

3.2. α-BTX conjugated with cND but not covalently binding

To examine the interaction of α-BTX and cNDs, suspensions of α-BTX, cND, and cND–α-BTX were loaded onto SDS-PAGE analysis. The amino acid sequence and molecular weight of α-BTX were shown as a 7.983 kD protein, which contained 74 amino acids [29]. After electrophoresis using SDS-PAGE, the molecular weight of α-BTX was ~8 kD in the gel (figure 2(A)). The cND particles did not present on the SDS-PAGE gel (figure 2(A)). The sample of cND–α-BTX also presented the α-BTX protein band (figure 2(A)). In addition, we manipulated α-BTX released from cND–α-BTX complexes. The molecular weight of α-BTX was obtained by MALDI/TOF-MS analysis. Figure 2(B) shows that the peak at m/z 8005 was the pattern of the α-BTX protein ion from the α-BTX separated samples.

3.3. Dual fluorescence imaging of α-BTX

The tetramethylrhodamine-labeled alpha-bungarotoxin (α-BTX-TMR) was incubated with cND particles and then subjected to laser scanning confocal microscopy. The cND particles exhibited green fluorescence at 510–530 nm after 488 nm excitation (figure 3, left pictures). The red fluorescence of TMR (excitation wavelength: 543 nm; emission wavelength: 560–580 nm) represented the location of α-BTX proteins (figure 3, middle pictures). Moreover, the merged pictures showing yellow color indicate the formation of cND–α-BTX-TMR complexes (figure 3, right pictures).

3.4. α-BTX binding on the cell membrane of lung A549 cancer cells

To determine the cND–α-BTX-TMR binding on targeting cells, the human A549 lung cancer cells were treated with these particles and were subjected to confocal microscopy. Both cND and cND–α-BTX-TMR particles were detected on cells that exhibited the green fluorescence from cND signals (figures 4(A) and (B)). The cND particles were taken up into cells but cND–α-BTX-TMR located on the cell membrane of A549 cells (figure 4(A)). The red fluorescence of TMR from cND–α-BTX-TMR indicated that α-BTX bound on the cell membrane of A549 cells. The black spots of cND–α-BTX-TMR complexes were also observed by phase contrast image (figure 4(B), left). The yellow color also indicated that the cND–α-BTX-TMR complexes were located on the cell membrane of A549 cells (figure 3, right picture).

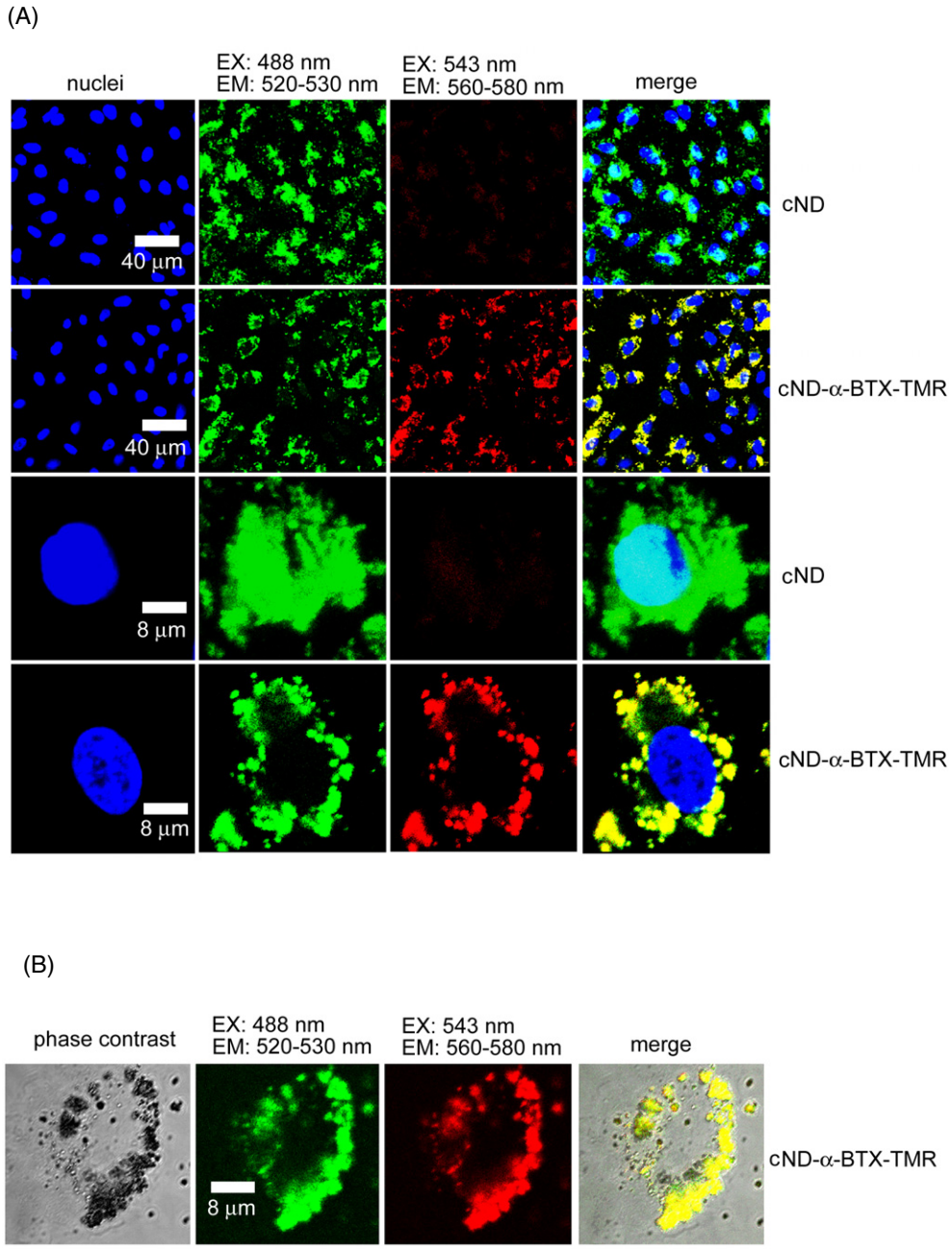

Figure 4. Detection of cND and cND–α-BTX-TMR in A549 cells by laser scanning confocal microscopy. (A) and (B), A549 cells were treated with 100 μg ml^{-1} cND or cND–α-BTX-TMR for 4 h and then had 20 h recovery. After cell fixation, the nuclei were stained with Hoechst 33258, which displayed blue fluorescence. The cND particles exhibited the green fluorescence at 510–530 nm after 488 nm excitation. The red fluorescence of TMR was excited with wavelength 543 nm and the emission was collected in the range of 560–580 nm. The black spots of cND–α-BTX-TMR complexes were observed by phase contrast. The yellow color in the merged pictures indicated the location of cND–α-BTX-TMR.

3.5. Quantification of cND and cND–α-BTX in A549 cells by flow cytometry

To quantify the level of cNDs and cND–α-BTX binding to A549 cells, the cells were treated with these particles and analyzed by flow cytometry. The fluorescence intensities were increased in A549 cells following treatment with 50 μg ml^{-1} cND or cND–α-BTX (figure 5(A)). The fluorescence intensity was significantly increased ∼2-fold after treatment with cNDs and cND–α-BTX (figure 5(B)). However, the fluorescence intensity of cND was similar to that of cND–α-BTX in A549 cells (figure 5(B)).

3.6. cND–α-BTX-TMR binding to α7-nAChR on cell membrane of Xenopus laevis's oocytes

The human α7-nAChR was expressed on *Xenopus laevis's* oocytes as described in Experimental Details section. The cND particles or cND–α-BTX-TMR bound to oocyte were observed by confocal microscopy. As shown in figure 6, the green fluorescence indicated nanodiamond's signal presenting

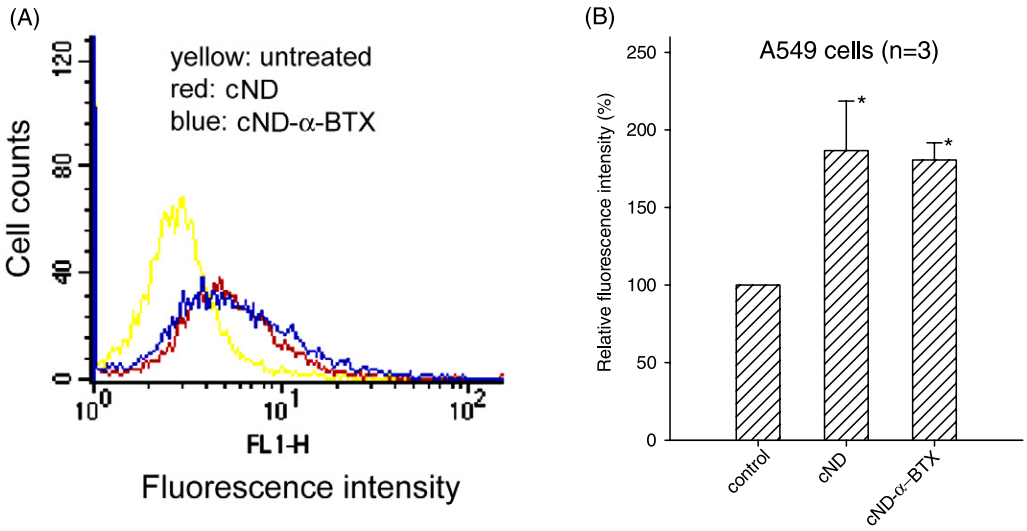

Figure 5. Quantified fluorescence intensities of cND and cND–α-BTX in A549 cells by flow cytometry. (A) A549 cells were treated with or without 100 μg ml^{-1} cND or cND–α-BTX for 4 h and then had 20 h recovery. At the end of treatment, the cells were trypsinized and then subjected to flow cytometry analyses. (B) The fluorescence intensity was quantified by a CellQuest software of the flow cytometer. The bar represents mean $\pm$S.E. $^{*}p < 0.05$ indicates significant difference between untreated and treated samples.

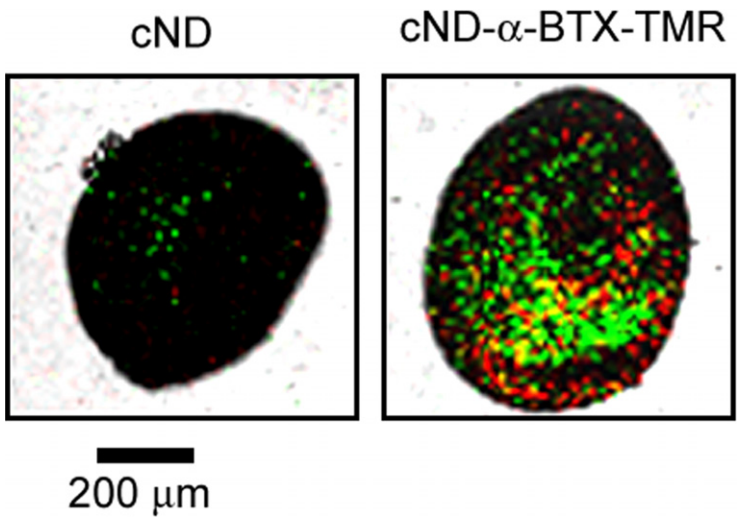

Figure 6. Observation of cND–α-BTX binding on the α7-nAChR-expressed oocytes. The oocytes from *Xenopus laevis* were injected with the α7-nAChR RNA using a nanoinjector. After incubation with cNDs or cND–α-BTX, the oocytes were fixed with 4% paraformaldehyde and were examined under laser scanning confocal microscopy. The green spots indicate the location of cND particles after 488 nm excitation and exhibited emission at 510–530 nm. The red fluorescence of TMR was excited with wavelength 543 nm and the emission was collected in the range of 560–580 nm. The yellow spots indicate the location of cND–α-BTX-TMR.

on the α7-nAChR-expressed oocytes. A few cND particles were located on the cell membrane of oocytes following incubation with 100 μg ml^{-1} cND for 10 min (figure 6, left). However, treatment with 100 μg ml^{-1} cND–α-BTX-TMR for 10 min caused high fluorescence intensities of cND and TMR (figure 6, right).

3.7. cND–α-BTX inhibits the choline-evoked inward currents by α7-nAChR on Xenopus laevis's oocytes

The effects of cND and cND–α-BTX on the α7-nAChR expressed in oocyte were measured by two-electrode voltage-clamp recording. The apparatus of two-electrode voltage-clamp recording is shown in figure 7(A). Representative tracings from a continuous recording showed choline-induced inward currents before, during (filled bars) and after 5 min administrations of cND or cND–α-BTX treatment. Treatment with 12 μg ml^{-1} cND did not affect the inward current induced by choline at 0.3 mM; however, 12 μg ml^{-1} cND–α-BTX (containing 30 nM α-BTX) significantly inhibited α7-nAChR-mediated current (figure 7(B)). The inhibition of choline-induced inward currents by cND–α-BTX binding on α7-nAChR was irreversible after the addition of fresh choline solution (data not shown). Quantification of current signals showed that cND had little effect on the choline-evoked inward currents (figure 7(C)). In contrast, cND–α-BTX reduced the

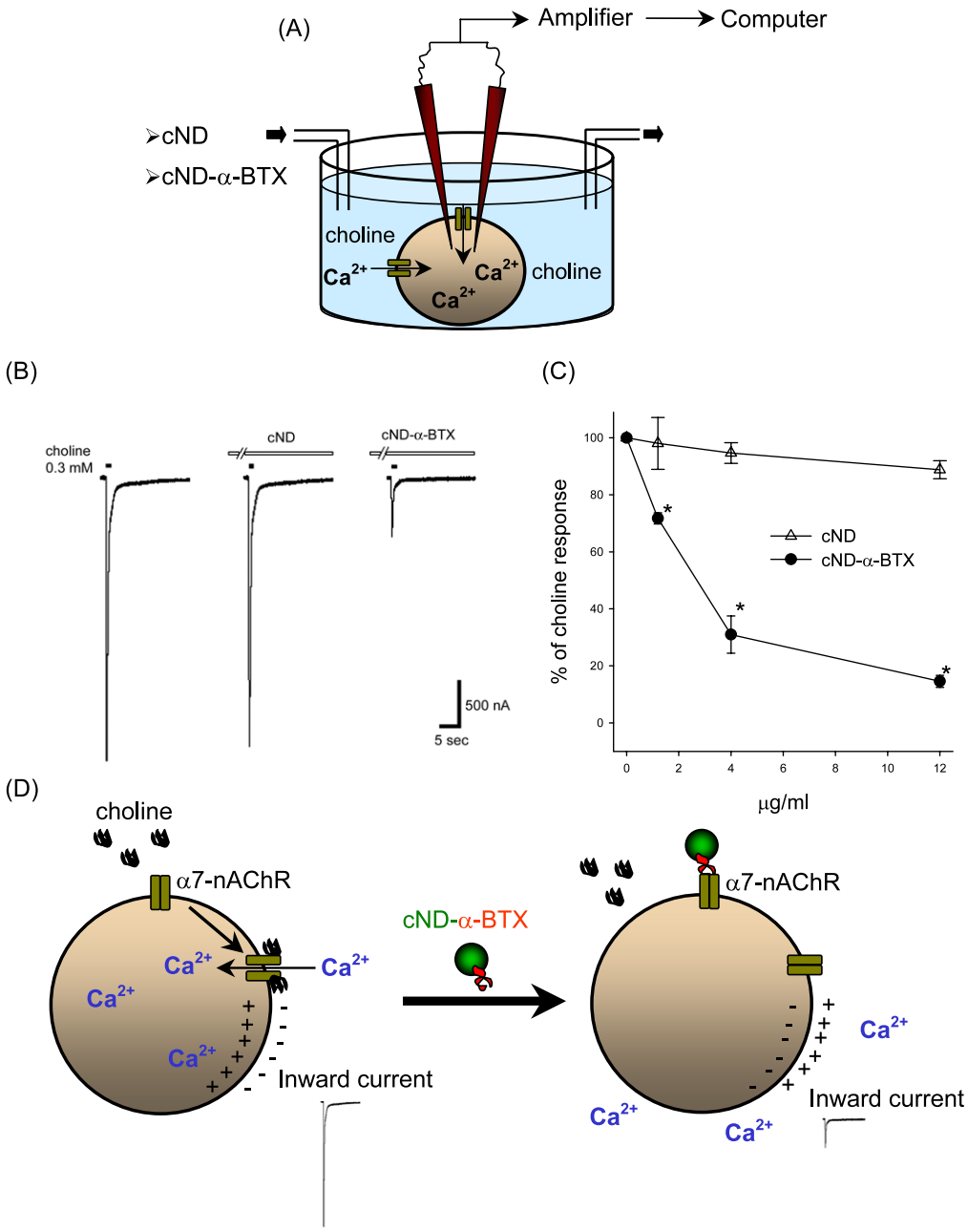

Figure 7. Effect of cND and cND–α-BTX on the choline-evoked inward current in the α7-nAChR-expressed oocytes. (A) The apparatus of the choline-evoked inward current in the α7-nAChR-expressed oocytes. (B) Oocytes were injected with the α7-nAChR RNA by using a nanoinjector. After microinjection, the effects of choline, cND, and cND–α-BTX on the α7-nAChR-expressed oocytes were measured by two-electrode voltage-clamp recording. Representative tracings from a continuous recording showing choline-induced inward currents before, during, and after 5 min administrations of cND or cND–α-BTX (12 μg ml^{-1}) treatment. (C) Summary of recordings showing normalized nicotinic responses after 5 min administrations of varied concentrations of cND or cND–α-BTX (0, 1.2, 4, 12 μg ml^{-1}). Data points were means $\pm$S.E from 3–4 successive recordings. $^{*}p < 0.05$ indicates significant difference between cND and cND–α-BTX. (D) A model presenting the choline-binding to α7-nAChR for evoking inward currents with Ca^{2+} influx into oocyte. The green color indicates a cND particle. The red color indicates the α-BTX protein. Choline evoked the inward current (Ca^{2+} influx into oocyte) by binding to the protein subunits of α7-nAChR on the cell membrane. The choline-evoked α7-nAChR-mediated inward current was blocked by cND–α-BTX.

α7-nAChR-mediated responses in a concentration-dependent manner (figure 7(C)).

4. Discussion

This is the first report to indicate that cND-conjugated α-BTX displays the biological activity to block the function of α7-nAChR on targeting cells. Importantly, the imaging of α-BTX revealed by conjugated nanodiamonds on target cells can be detected and quantified by laser scanning confocal microscopy and flow cytometry. This study provides a visual system by cND conjugation with a biological molecule, which is promising for biological applications.

Manipulation of biological molecules by conjugation with nanoparticles is a useful tool for both bio-imaging and drug delivery [1, 2, 5, 6]. Qdots emit fluorescent properties without photobleaching, which have been used in bio-imaging and bio-detection [1, 3, 6]. However, Qdots usually consist of heavy metals such as cadmium, which is well-known to cause a human carcinogen that is of serious concern for medical applications. Previously, we reported that cND particles did not induce cytotoxicity or alter the protein expression profile in human lung cells [8]. Moreover, these particles can be detected by their intrinsic fluorescence and without obvious photobleaching [7, 9]. Therefore, cND provides an ideal alternative nanomaterial because of its biocompatible and spectroscopic detectable properties.

The surface of nanodiamonds provides a unique platform for conjugation of biological molecules after chemical modifications [10, 11]. These cND particles have a high appetence for protein binding [7, 12]. It has been reported that proteins can be adsorbed by cND via electrostatic interaction, which is strong and suitable for MALDI/TOF-MS analysis [12]. Indeed, cND particles have shown to possess high affinity for binding with α-BTX proteins. The average size of cND–α-BTX complexes is ~300 nm. The green fluorescence of cND particles combining with the red fluorescence of TMR-labeled α-BTX presented a yellow color at the same location, which that indicated α-BTX proteins were conjugated with cND particles. However, α-BTX can be dissociated from cND–α-BTX complexes presenting on the SDS-PAGE gel and MALDI/TOF-MS spectrum. The PI (isoelectric point) value of α-BTX is 8.38 in pH 7.4–7.6 (physiological condition used in this study) carrying positive charge. The negative charge of cND particles from the carboxyl group ($-COO^-$) is electrostatic with the positive charge of α-BTX from the amino group ($-NH_3^+$) in physiological pH condition. Therefore, the conjugation of cND and α-BTX is due to the electrostatic force but not the covalent bonding. In general, electrostatic bonding is very strong. Furthermore, cND–α-BTX reduced the α7-nAChR-mediated responses in a concentration-dependent manner. Therefore, the binding affinity of α-BTX and cND is strong and suitable for bio-applications in those physiological conditions. Although the binding stability of the alpha-BTX-cND complex was not studied in this work, the bonding between cND and α-BTX under different pH and buffer conditions is currently under investigation.

It has been shown that α7-nAChR regulates a wide range of physiological functions [17, 26–28]. The α7-nAChRs located on the cellular membrane to mediate cation influx, particularly Ca^{2+} in flux [22–25]. The specific α7-nAChR is expressed in several human lung cancer cell lines, including A549 cells [19–21]. Moreover, the neuronal α7-nAChR displays neuroprotection [17, 27]. α-BTX is a polypeptide composed of 74 amino acids (~8 kDa) [29]. It is a neurotoxin that binds α7-nAChR to induce neuronal damages [17, 18]. Furthermore, α-BTX can block α7-nAChR-mediated downstream signaling pathways [18, 19, 28, 30]. We provided two models of the exogenously expressed α 7-nAChR in *Xenopus* oocyte and the endogenous α7-nAChR in A549 cells and performed cND–α-BTX complexes binding to α7-nAChR of target cells. Interestingly, cND-conjugated α-BTX preserves the biological activity in blocking choline-evoked inward currents in the α7-nAChR-expressed oocyte.

In conclusion, we propose a model of a visual system by cND-conjugated α-BTX that preserves the physiological activity of blocking the function of α7-nAChR on targeting cells (figure 7(D)). Although this study provides the model of cND–α-BTX for imaging in human cancerous cell and oocyte *in vitro*, it is expected that the biological applications of nanodiamond-conjugated bio-molecules will be widely used in a variety of systems including bio-imaging, bio-detection, and bio-sensing.

Acknowledgments

This work was supported by grants from the National Science Council, ROC (NSC 95-2120-M-259-002, NSC 95-2120-M-259-003, NSC 95-2745-B-320-004-URD), and Tzu Chi University (TCMRC-C95005-01).

References

[1] Akerman M E, Chan W C, Laakkonen P, Bhatia S N and Ruoslahti E 2002 Nanocrystal targeting *in vivo Proc. Natl Acad. Sci. USA* **99** 12617–21

[2] Michalet X, Pinaud F F, Bentolila L A, Tsay J M, Doose S, Li J J, Sundaresan G, Wu A M, Gambhir S S and Weiss S 2005 Quantum dots for live cells, *in vivo* imaging, and diagnostics *Science* **307** 538–44

[3] Gao X, Cui Y, Levenson R M, Chung L W and Nie S 2004 *In vivo* cancer targeting and imaging with semiconductor quantum dots *Nat. Biotechnol.* **22** 969–76

[4] Souza G R, Christianson D R, Staquicini F I, Ozawa M G, Snyder E Y, Sidman R L, Miller J H, Arap W and Pasqualini R 2006 Networks of gold nanoparticles and bacteriophage as biological sensors and cell-targeting agents *Proc. Natl Acad. Sci. USA* **103** 1215–20

[5] Farokhzad O C, Cheng J, Teply B A, Sherifi I, Jon S, Kantoff P W, Richie J P and Langer R 2006 Targeted nanoparticle–aptamer bioconjugates for cancer chemotherapy *in vivo Proc. Natl Acad. Sci. USA* **103** 6315–20

[6] Dahan M, Levi S, Luccardini C, Rostaing P, Riveau B and Triller A 2003 Diffusion dynamics of glycine receptors revealed by single-quantum dot tracking *Science* **302** 442–5

[7] Chao J I, Perevedentseva E, Chung P H, Liu K K, Cheng C Y, Chang C C and Cheng C L 2007 Nanometer-sized diamond particle as a probe for biolabeling *Biophys. J.* **93** 2199–208

[8] Liu K K, Cheng C L, Chang C C and Chao J I 2007 Biocompatible and detectable carboxylated nanodiamond on human cell *Nanotechnology* **18** 325102

[9] Yu S J, Kang M W, Chang H C, Chen K M and Yu Y C 2005 Bright fluorescent nanodiamonds: no photobleaching and low cytotoxicity *J. Am. Chem. Soc.* **127** 17604–5

[10] Yang W *et al* 2002 DNA-modified nanocrystalline diamond thin-films as stable, biologically active substrates *Nat. Mater.* **1** 253–7

[11] Carlisle J A 2004 Precious biosensors *Nat. Mater.* **3** 668–9

[12] Kong X L, Huang L C, Hsu C M, Chen W H, Han C C and Chang H C 2005 High-affinity capture of proteins by diamond nanoparticles for mass spectrometric analysis *Anal. Chem.* **77** 259–65

[13] Ushizawa K, Sato Y, Mitsumori T, Machinami T, Ueda T and Ando T 2002 Covalent immobilization of DNA on diamond and its verification by diffuse reflectance infrared spectroscopy *Chem. Phys. Lett.* **351** 105–8
[14] Huang L C and Chang H C 2004 Adsorption and immobilization of cytochrome c on nanodiamonds *Langmuir* **20** 5879–84
[15] Kossovsky N, Gelman A, Hnatyszyn H J, Rajguru S, Garrell R L, Torbati S, Freitas S S and Chow G M 1995 Surface-modified diamond nanoparticles as antigen delivery vehicles *Bioconjug. Chem.* **6** 507–11
[16] Cheng C Y, Perevedentseva E, Tu J S, Chung P H, Chenga C L, Liu K K, Chao J I, Chen P H and Chang C C 2007 Direct and *in vitro* observation of growth hormone receptor molecules in A549 human lung epithelial cells by nanodiamond labeling *Appl. Phys. Lett.* **90** 163903
[17] Shaw S, Bencherif M and Marrero M B 2002 Janus kinase 2, an early target of alpha 7 nicotinic acetylcholine receptor-mediated neuroprotection against Abeta-(1-42) amyloid *J. Biol. Chem.* **277** 44920–4
[18] Wang Y, Pereira E F, Maus A D, Ostlie N S, Navaneetham D, Lei S, Albuquerque E X and Conti-Fine B M 2001 Human bronchial epithelial and endothelial cells express alpha7 nicotinic acetylcholine receptors *Mol. Pharmacol.* **60** 1201–9
[19] West K A, Brognard J, Clark A S, Linnoila I R, Yang X, Swain S M, Harris C, Belinsky S and Dennis P A 2003 Rapid Akt activation by nicotine and a tobacco carcinogen modulates the phenotype of normal human airway epithelial cells *J. Clin. Invest.* **111** 81–90
[20] Hsu S H, Tsou T C, Chiu S J and Chao J I 2005 Inhibition of alpha7-nicotinic acetylcholine receptor expression by arsenite in the vascular endothelial cells *Toxicol. Lett.* **159** 47–59
[21] Dasgupta P, Kinkade R, Joshi B, Decook C, Haura E and Chellappan S 2006 Nicotine inhibits apoptosis induced by chemotherapeutic drugs by up-regulating XIAP and survivin *Proc. Natl Acad. Sci. USA* **103** 6332–7
[22] Bitner R S and Nikkel A L 2002 Alpha-7 nicotinic receptor expression by two distinct cell types in the dorsal raphe nucleus and locus coeruleus of rat *Brain Res.* **938** 45–54
[23] Castro N G and Albuquerque E X 1995 Alpha-bungarotoxin-sensitive hippocampal nicotinic receptor channel has a high calcium permeability *Biophys. J.* **68** 516–24
[24] Albuquerque E X, Alkondon M, Pereira E F, Castro N G, Schrattenholz A, Barbosa C T, Bonfante-Cabarcas R, Aracava Y, Eisenberg H M and Maelicke A 1997 Properties of neuronal nicotinic acetylcholine receptors: pharmacological characterization and modulation of synaptic function *J. Pharmacol. Exp. Ther.* **280** 1117–36
[25] Papke R L, Bencherif M and Lippiello P 1996 An evaluation of neuronal nicotinic acetylcholine receptor activation by quaternary nitrogen compounds indicates that choline is selective for the alpha 7 subtype *Neurosci. Lett.* **213** 201–4
[26] Trombino S, Cesario A, Margaritora S, Granone P, Motta G, Falugi C and Russo P 2004 Alpha7-nicotinic acetylcholine receptors affect growth regulation of human mesothelioma cells: role of mitogen-activated protein kinase pathway *Cancer Res.* **64** 135–45
[27] Kihara T, Shimohama S, Sawada H, Honda K, Nakamizo T, Shibasaki H, Kume T and Akaike A 2001 Alpha 7 nicotinic receptor transduces signals to phosphatidylinositol 3-kinase to block A beta-amyloid-induced neurotoxicity *J. Biol. Chem.* **276** 13541–6
[28] Mozayan M, Chen M F, Si M, Chen P Y, Premkumar L S and Lee T J 2006 Cholinesterase inhibitor blockade and its prevention by statins of sympathetic alpha7-nAChR-mediated cerebral nitrergic neurogenic vasodilation *J. Cereb. Blood Flow Metab.* **26** 1562–76
[29] Mebs D, Narita K, Iwanaga S, Samejima Y and Lee C Y 1971 Amino acid sequence of-bungarotoxin from the venom of Bungarus multicinctus *Biochem. Biophys. Res. Commun.* **44** 711–6
[30] Zhang Q, Tang X, Zhang Z F, Velikina R, Shi S and Le A D 2007 Nicotine induces hypoxia-inducible factor-1alpha expression in human lung cancer cells via nicotinic acetylcholine receptor-mediated signaling pathways *Clin. Cancer Res.* **13** 4686–94